Untangling intercropping in heterogeneous smallholder maize-cassava farming systems with remote sensing

Felicia O. Akinyemi[a,b,1]*, Philippe Rufin[c,d], Esther Shupel Ibrahim[d,e,f], Patrick Hostert[d,g], Lucia O. Ogunsumi[h], Olugbenga A. Egbetokun[h], Chinwe Ifejika Speranza[a]

[a]Land Systems and Sustainable Land Management, Institute of Geography, University of Bern, Hallerstrasse 12, 3012 Bern, Switzerland; felicia.akinyemi@unibe.ch; chinwe.ifejika.speranza@unibe.ch

[b]Geomatics, Department of Environmental and Life Sciences, Karlstads University, Universitetsgatan 2, 651 88 Karlstad, Sweden; felicia.akinyemi@kau.se

[c]Earth and Life Institute, UCLouvain, Place Louis Pasteur 3, 1348 Louvain-La-Neuve, Belgium; philippe.rufin@uclouvain.be

[d]Geography Department, Humboldt-Universität zu Berlin, Unter den Linden 6, 10099 Berlin, Germany; esther.shupel.ibrahim@hu-berlin.de; patrick.hostert@geo.hu-berlin.de

[e]Leibniz Centre for Agricultural Landscape Research, Eberswalder Straße 84, 15374 Müncheberg, Germany

[f]National Centre for Remote Sensing, Jos, Rizek Village Jos Eat LGA, P.M.B. 2136 Jos, Plateau State, Nigeria

[g]IRI THESys – Integrative Research Institute on Transformations of Human-Environment Systems, Humboldt-Universität zu Berlin, Unter den Linden 6, 10099 Berlin, Germany

[h]Institute of Agricultural Research and Training, Obafemi Awolowo University, Moor Plantation, Ibadan, Nigeria; lucyogunsumi2011@gmail.com; oaegbetokun@gmail.com

This paper is a non-peer reviewed preprint submitted to EarthArXiv. It has been submitted to the Remote Sensing of Environment for peer review.

[1] *Corresponding author. Land Systems and Sustainable Land Management, Institute of Geography, University of Bern, Hallerstrasse 12, 3012 Bern, Switzerland, akinyemi.felicia @gmail.com +41 779693968.

Abstract

Earth observation approaches for large-scale crop monocultures are often not transferable to heterogeneous smallholder systems. Key challenges in this regard are intercropping, high intra-field crop type variability, wide sowing windows, presence of non-crop vegetation and small but variable field sizes. Currently, studies on smallholder agriculture mainly focus on specific crops and seldom account for crop mixtures or multiple growing cycles. Moreover, our knowledge about ongoing processes of farm consolidation and effects on intercropping remains limited due to the absence of spatially detailed information on field size. We mapped monocropping and maize-cassava intercropping in 2022/2023 and the relationship with field sizes. We combined Sentinel-1 radar and optical Sentinel-2 time series to classify farming systems across two growing cycles in the Guinea Savannah of southwest Nigeria. We tested spectral-temporal features at monthly and bimonthly intervals for the growing season and off-season. We used deep transfer learning to fine-tune a pre-trained convolutional neural network designed for crop field delineation. Using very high resolution imagery (0.6 m) for a regularly distributed sample across the study region (n=2,333), mean overall accuracy based on k-fold cross-validation was 0.79 (+/-0.02%), whereas User and Producer accuracies were above 0.70 for most classes. Sentinel-1 alone underperformed, while models using only Sentinel-2 had higher overall accuracies but suffered from cloud-induced data gaps. Field size estimation revealed a high spatial agreement with mean intersection over union scores of up to 0.73 in site-level field size estimation. Small and medium-sized fields were dominant. Monocropping was positively related to field sizes as larger monocropping fields of early-planted cassava, late-planted maize, yam and rice clustered in the North of our study region. In contrast, smaller intercropped fields of maize-cassava mainly occurred in fragmented agricultural landscapes with ample natural vegetation. Our approach demonstrates the potential of integrating radar and optical time series in cloud-prone regions for mapping crop mixtures in complex forest-agricultural mosaic landscapes during multiple growing cycles. Our study provides a valuable workflow for producing timely information for the quantification of crop production in heterogeneous smallholder farming systems.

Graphical abstract

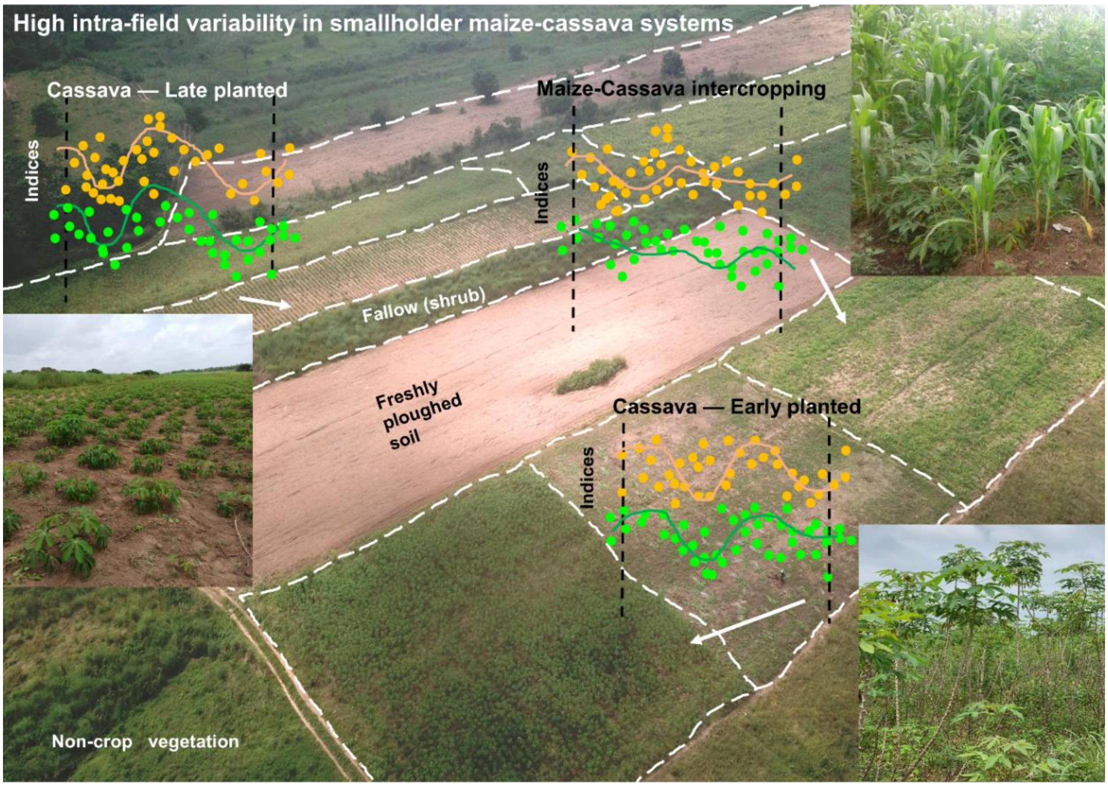

Keyword

Spectral-temporal features, smallholder, mixed farming, Sentinel 1 - 2, Random Forest, Automated field delineation

Highlights

- Mapped intercropping in mixed crop farming and double growing cycles in smallholder farming systems
- Best model for predicting crop types combined Sentinel-1 at monthly and Sentinel-2 at bimonthly intervals
- Mapping early and late planted crops better reflects the local agroclimatic context
- Detailed field size delineation and estimates were efficiently obtained with deep transfer learning
- Monocropping was positively related to field size in the Nigerian lower Guinea Savannah

1. Introduction

Remote Sensing provides timely and cost-efficient input for agricultural monitoring across large regions for pre- and within-growing season decision support (Johnson, 2014). Most approaches currently applied for mapping crop types were developed for large-scale crop monocultures, especially in industrialized economies (Fritz et al., 2019; Taiwo et al., 2023; Becker-Reshef et al., 2023). However, these approaches have limited applicability in heterogeneous agricultural systems such as those dominating smallholder agriculture worldwide, especially in developing countries. Smallholder farms are often heterogeneous and small, loosely defined by farm sizes of < 2 - 5 ha (FAO, 2014; Samberg et al., 2016; Fatunbi et al., 2020; Lowder et al., 2021). As smallholder agriculture produces about 30-34% of the global food supply, it is vital to reaching the Sustainable Development Goal (SDG) 2, which is concerned with ending hunger, achieving food security, improving nutrition and promoting sustainable agriculture (United Nations, 2015; FAO, 2016; Ricciardi et al., 2018).

Mapping crop types and their associated cropping patterns (i.e., mono- and mixed cropping) in smallholder contexts from remote sensing is challenging, especially for intercropping, a type of mixed farming characterized mainly by the simultaneous presence of multiple crops (Akinyemi, 2017; Kinyua et al., 2023). Intercropping is a traditional method of agricultural intensification aimed at increasing food production per unit of land and minimizing the risks of crop failure due to impacts such as drought and pests (Olasantan et al., 1996; Ayoola and Makinde, 2007; Bouws and Finckh, 2008; Nwokoro et al., 2021). Aside from the tendency for smallholder farms to be heterogeneous and small, notable constraining factors are the high intra-field variability in crop types and non-crop vegetation, the wide sowing windows and the lack of reference data for the mixed farming systems (Ibrahim et al., 2021). As elsewhere in the tropics, the lack of cloud-free optical images to map smallholder agriculture during much of the growing season necessitates combining images from different sensors, which is helpful for crop type mapping in some smallholder contexts (e.g., Kpienbaareh et al., 2019; Rao et al., 2021; Ren et al., 2022). These factors compound the difficulty of mapping crop types and intercropping, especially distinguishing the phenology of multiple crops at different growth stages. Consequently, regional-scale crop type mapping approaches in intercropping systems have mainly focused on specific crops and often do not consider crop mixtures or multiple growing cycles.

This study considers the Lower Guinea Savannah (LGS), a predominantly smallholder agricultural region in the southwest of Nigeria. Historically, agricultural programmes implemented in this region have aimed at harnessing more arable lands for agriculture, hence the link to cropland expansion (Ekong, 1983; Akinyemi and Ifejika Speranza, 2022). Examples of such programmes are the farm settlement scheme of the 1950s, providing incentives for land and farm input (Ministry of Agriculture and Natural Resources, 1959) and the trade liberalization policy of the 1980s and 1990s prioritizing smallholder export-oriented cash crop production (Akinyemi, 2013). With the co-existence of various farming systems, the LGS presents a good case to predict crop types and map intercropping during multiple growing cycles in smallholder regions.

Despite intercropping being the dominant agricultural practice among smallholder farmers in Nigeria, as elsewhere in Africa where small- and large scale commercial monocropping systems using mechanization are emerging (Muyanga et al., 2019; Omotilewa field size is increasing (Ibrahim et al., 2021; Chiaka et al., 2022). Using the classes in the global study of field size distribution (Lesiv et al., 2019), Nigeria has 56% of very small fields (<0.64 ha), 31% small fields (0.64 - 2.56 ha), 11% medium fields (2.56 - 16 ha), 2% large fields (16 - 100 ha) and 1% very large fields (>100 ha). However, spatially explicit information on field size and the relationship to cropping patterns remains largely unknown. Therefore, we tested the detection of individual smallholder fields at very high spatial resolution utilizing deep transfer learning and relating field size to cropping systems. We hypothesized that field size is related to the cropping system, with larger fields more likely being monocropped and smaller fields instead being cultivated in a mixed farming regime. This study's objectives were as follows:

- Develop a framework most suitable for predicting and mapping multiple crops and intercropping by combining spectral-temporal features of S1 and S2
- Map multiple crops and differentiate the cropping patterns (i.e., mono- and intercropping), considering there are two growing cycles per year
- Assess how field size relates to cropping patterns in smallholder farming systems

2. Data and methods

2.1 Study region

As the most populated African country, Nigeria is experiencing a food crisis with 17 million people estimated to be critically food insecure in 2022 due to natural disasters and social conflicts (Bizikova et al., 2022; Famine Early Warning System Network, 2023a, 2023b). The country comprises several agroecological zones (Fig. 1a). In the ultra-humid mangrove, freshwater swamps and rainforests, rainfall exceeds 2,000 mm yr^{-1} and monthly min/max temperature (tmin/tmax) is 23/33°C. In contrast, the Guinea Savannah has ca.1,000 mm yr^{-1} rainfall and monthly tmin/tmax of 20/37°C, the Sudan Savannah and Sahel Savannah are limited to 440 – 600 mm yr^{-1} rainfall and tmin/tmax of 13 – 40°C (Iloeje, 2001). Agriculture in Nigeria is organized into five zones, these are northwest, northeast, central, southwest and southeast. LGS (our study region) falls mainly in the lower Guinea Savannah of the southwest agricultural zone. Elevation peaks at 532 m (Fig. 1b). There are two growing seasons in LGS, these are the early planting season and the late planting season. The early planting season commences in March when rainfall starts, lasting until July. The late planting season begins in August and continues until rainfall cessation in October or November.

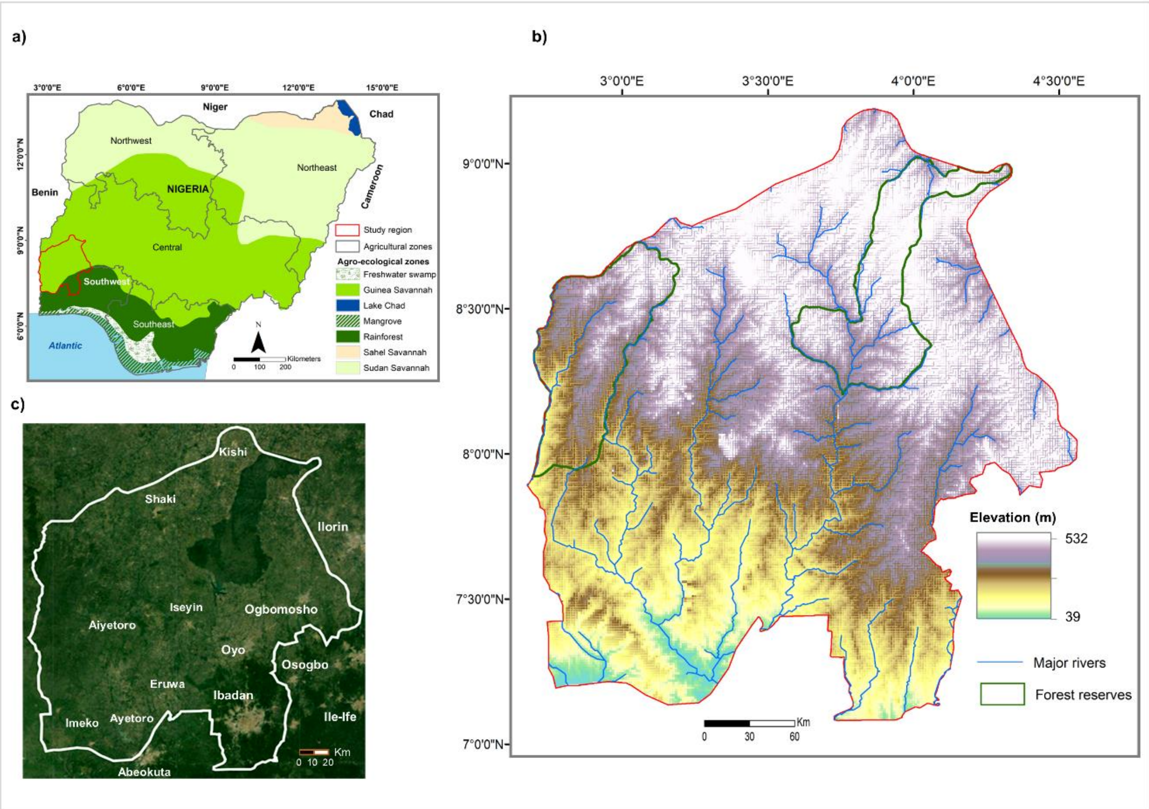

Fig. 1. Study location a) The lower Guinea savannah in the Nigerian southwest agricultural zone, b) Biophysical context of the study region (Data source: Elevation – USGS 30 arc-second GTOPO30, rivers - FAO rivers in Africa, forest reserve boundaries - Protectedplanet), c) Depicting major settlements in the study region on a natural colour composite (Google Earth Engine 2022).

Major farming systems that were identified as essential to meet the domestic food requirement are maize, cassava, yam and rice. Some minority crops were also considered (e.g., cocoyam, sweet potato, cowpea). Table 1 shows the cropping calendar for these crops in 2022 when fieldwork was conducted. To better capture the two growing cycles in our modelling for 2022, we categorized maize and cassava into early and late planting. With the possibility that a field is cultivated during both planting seasons, the crop grown during each growing cycle is mapped and referred to as early maize, late maize, early cassava and late cassava. It is also possible that what was detected on the field during the early planting season was late cassava planted the previous year during the early planting season. Such late cassava planted during the last year is harvested after rainfall starts during the early planting season of the subsequent year.

Table 1. Cropping calendar for crops in eight farming systems in 2022

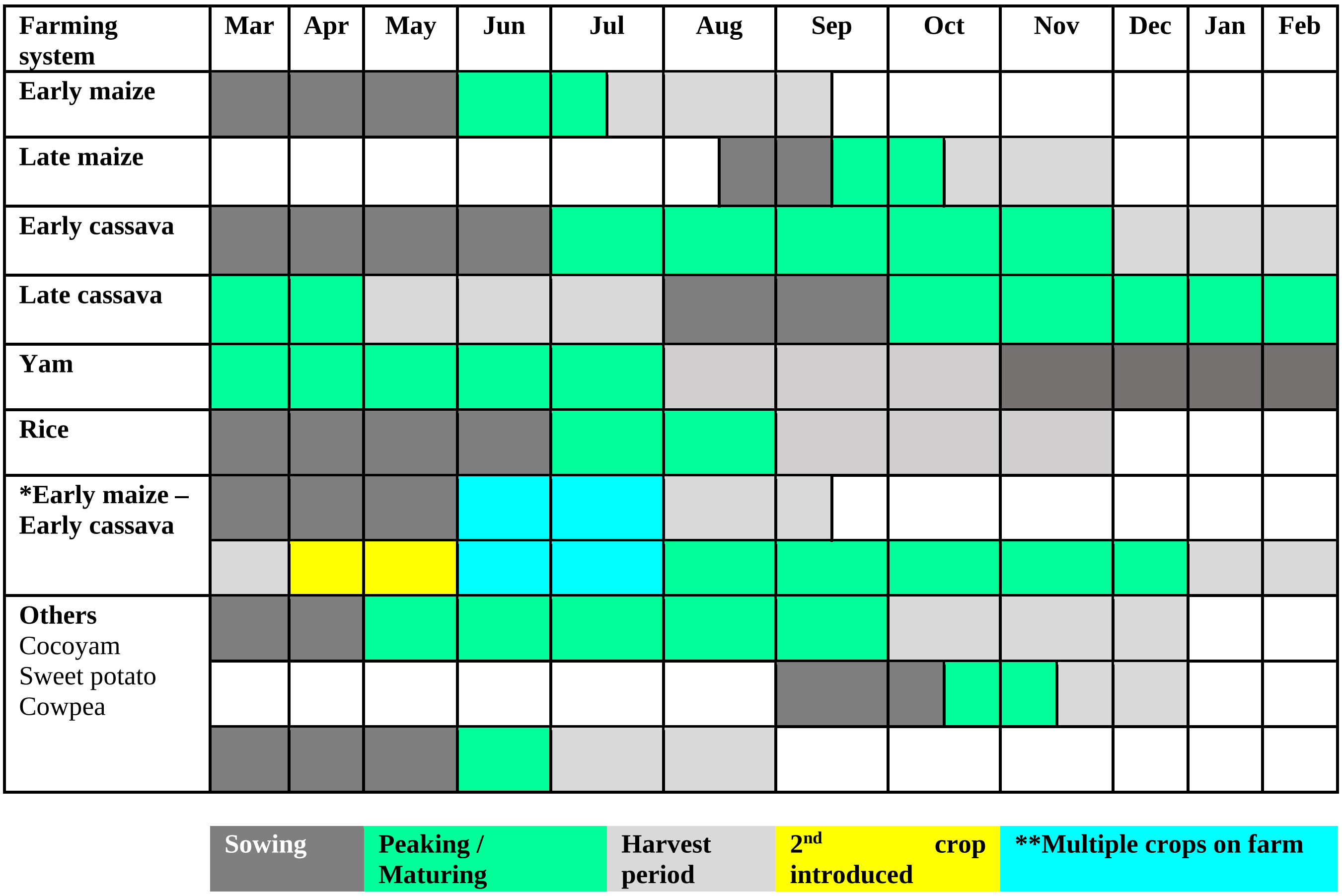

Note: *The remains of the maize stems that were left standing after harvest in cassava fields indicate maize-cassava mixed farming systems. **The critical windows in the intercropping system, whereby both crops are present on the field, must be detected to profile the crop phenology properly. Information sources: oral interviews with Agricultural Development Programme officials, farmers and the USDA crop calendar for Nigeria [http://fas.usda.gov/pecad/pecad.html Accessed 09 March 2023]

2.2 Mapping of farming systems

2.2.1 Workflow

The workflow comprises three main components (Fig. 2): a) A satellite remote sensing-based image data preprocessing framework to create consistent spectral-temporal features of S1 and S2 for mapping multiple crops and intercropping, b) model parameterization, classification, iterative active learning to fine-tune model and k-fold cross validation, c) the reference data collection used for model training and iterative active learning. The entire workflow was developed in the Google Earth Engine Python Application Programming Interface (API) (Gorelick et al. 2017).

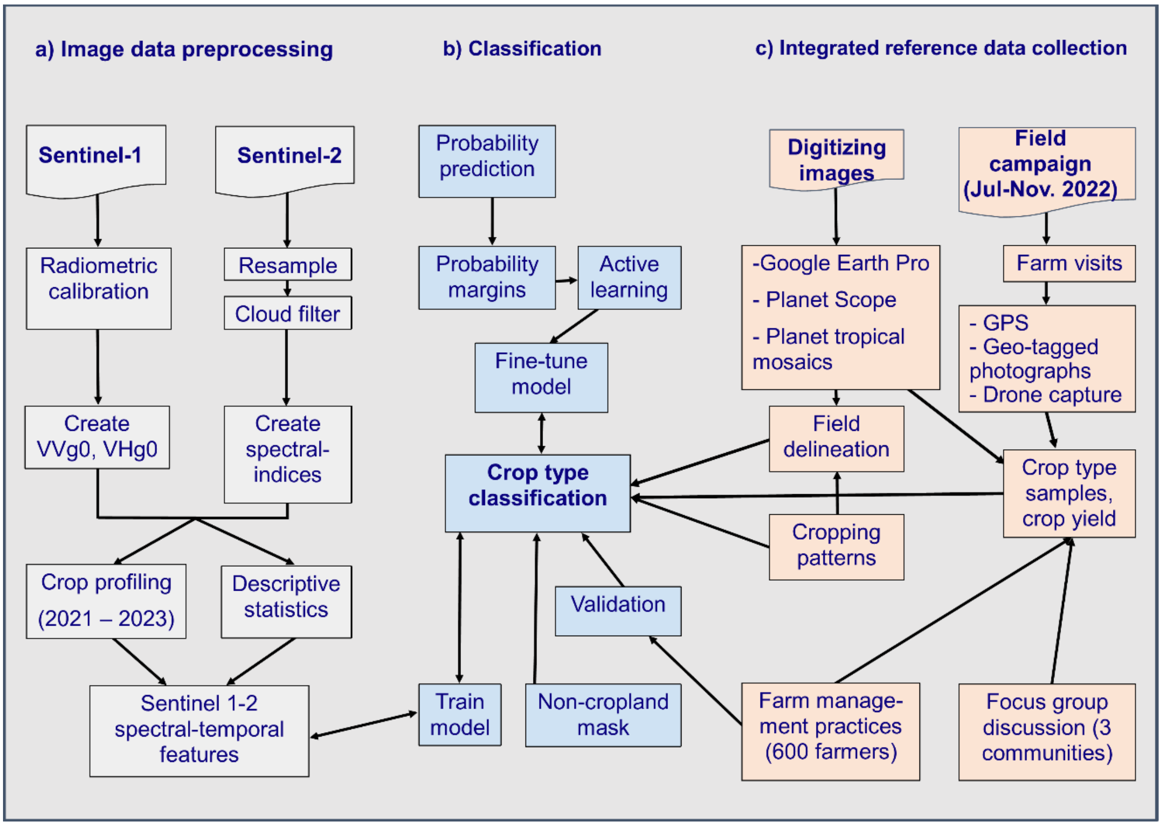

Fig. 2. Workflow describing tasks in image preprocessing, crop type classification, and reference data collection (remote sensing and place-based)

2.2.2 Remote sensing data and preprocessing

We used the S2A and S2B Level 2A image collection. All bands were resampled to 10m spatial resolution. The Normalized Difference Vegetation Index (NDVI), Normalized Difference Bare Index (NDBI) and the Normalized Difference Water Index (NDWI) were computed and included in the classification. Due to the prevalence of cloud cover during the growing season, we combined the S2 optical data with Synthetic Aperture Radar (SAR) data obtained from S1A. We used the S1A C-band Ground Range Detected image collection, providing image data which underwent thermal noise removal, radiometric calibration, and terrain correction using the European Space Agency S1 toolbox. We retained only images from ascending orbit to increase the consistency of the acquisition timing. We used the S1 Vertical transmit - Vertical receive (VV) and Vertical transmit - Horizontal receive (VH) backscatter values to generate VV gamma nought (VVg0) and VH gamma nought (VHg0) at 10m spatial resolution.

Both datasets were constrained to acquisitions between July 2021 and March 2023. The S1 time series was aggregated into bins for the entire study period. In contrast, due to incessant cloud cover during the rainy season, the S2 time series was constrained to the dry season, where observation density is comparably high. We aggregated S1 and S2 into bins with varying sensor constellations and temporal binning (Table 2). For each bin, we generated 25%, 50%, and 75% percentiles, interquartile mean (imean), interquartile range (iqr), and standard deviation (sd) of each band's surface reflectance or index values for S2. In contrast, for S1, we computed the average VHg0 and VVg0 and cross-polarization ratio (CR) as the ratio between VHg0 and VVg0 for each bin.

Table 2 Input features used for image classification experiments

No.	**Experiments**	**Number of features**	S1	S2
1	S1 bimonthly	27	bimonthly	
2	S2 bimonthly	396		bimonthly
3	S1 monthly	54	monthly	
4	S2 monthly	792		monthly
5	S1 monthly + S2 monthly	846	monthly	monthly
6	S1 bimonthly + S2 bimonthly	423	bimonthly	bimonthly
7	S1 monthly + S2 bimonthly	450	monthly	bimonthly

2.2.3 Reference data

Reference datasets required for model training and map accuracy assessment were acquired during field campaigns from July to November 2022. We used a stratified random sampling design to collect georeferenced data on crop types and cropping patterns (i.e., mono- or mixed cropping). The strata are maize, cassava, yam, rice, sweet potato, cocoyam, legume (e.g., cowpea, peanuts), maize-cassava, maize-legumes and horticulture (e.g., tomato, pepper and vegetable). Georeferenced samples were collected in Oyo and Ogun states, including geotagged photographs and Red, Green and Blue (RGB) images (2 cm) using an Unmanned Aerial Vehicle (UAV). Additional samples of crop types were digitized from Maxar images in Google Earth Pro. The Planet Tropical Normalized Analytic Monthly Monitoring Mosaics complimented with Level 1 PlanetScope surface reflectance scenes (3m) were used to cross-check these samples (Planet Team, 2022; Planet-Norway International Climate and Forests Initiative - Planet-NICFI, 2023). The reference datasets were compiled in QGIS 3.26 and ArcGIS 10.8. Digitized crop samples were used to augment the field data, especially for the yam and rice classes.

Eight target farming system classes were defined, indicating crop types, mixtures, and growing periods (Table 3). These classes were early maize, late maize, early cassava, late cassava, maize-cassava, yam, rice, and Others combining three minor crops. For classification, we used a stratified sample (n=996) of all samples (n=2,127) to reduce class imbalances.

Table 3. Farming systems and the number of samples in the model run before and after active learning (see section 2.2.4)

Farming system classes	**Description**	**Samples used**	**Active learning labels added**
Early maize	*Monocropping maize system planted in the early part of the first planting season.	118	8
Late maize	**Monocropping maize system planted late during the second planting season.	99	41
Early cassava	Monocropping system of cassava planted during the first planting season.	171	16
Late cassava	Monocropping system of cassava planted late during the second planting season.	132	6

Yam	Monocropping yam system, not including cocoyam.	167	41
Rice	Monocropping lowland rice grown on floodplains.	88	7
Maize-Cassava	The mixed farming system of early maize is intercropped with early cassava. ***Cassava is introduced one month after planting maize. Maize is harvested before the canopy closure of cassava.	151	29
Others	Cocoyam, sweet potato and cowpea.	70	0
Total		**996**	**148**

* The first planting season is from March to July. **The second planting season is from August to October. ***Farmers' description of their crop management practices.

We screened reference data by creating crop phenological profiles to aid in discriminating the identified farming systems from S1 and S2 images. Crop growth dynamics were inspected over time across multiple growing seasons from July 2021 to March 2023. This period was selected to better capture perennial crops (e.g., cassava) (Fig. 3). Crop profiles were created using S1 time series of VHg0 and VVg0, vegetation (e.g., NDVI), bare (e.g., NDBI) and moisture indices (e.g., NDWI) were created from S2 time series. Image availability per sensor is the data point in the graphs (Fig. 3). The availability of S2 images was limited during much of the growing seasons (i.e., March - October 2022) due to cloud cover and shadow. This screening aided in assessing the quality of the samples for each farming system class, especially where information on vegetation presence was needed to discriminate early cassava from maize-cassava class.

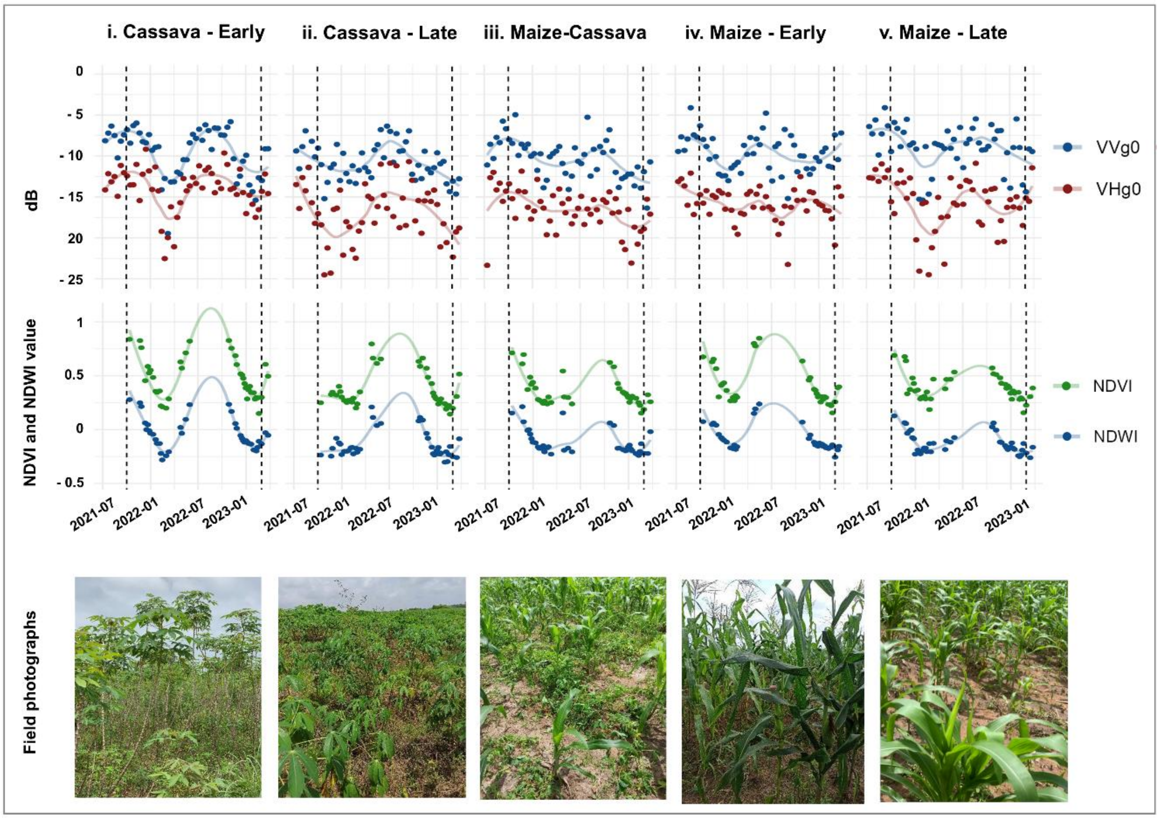

Fig 3. Crop profiling based on S1 and S2 time series. Valid observations were interpolated using locally weighted regression estimates (loess) to aid visual interpretation of phenological profiles.

2.2.4 Crop type classification

Crop type classification consisted of model training, iterative active learning to improve model performance, and predicting the farming system classes throughout the study region (Fig. 2b). We used the screened crop type samples to train the Random Forest model. Active learning was also conducted to fine-tune the model (Tuai et al., 2011; Strumpf et al., 2014; Rufin et al., 2022). Additional samples needed for active learning were created in areas of model uncertainty. Based on the level of model uncertainty, we generated a map of probability margins from the Random Forest class probabilities for the eight farming system classes (Fig. 2b). Probability margins represent the probability difference between the predicted class and the class with the second-highest probability value. Low probability margins indicate regions where the model is uncertain and can profit from additional training samples. We calculated class-wise 25% percentiles of probability margins and created a stratified random sample in the study area (n=60 per class). To avoid sampling isolated pixels, we performed a sieving operation to sample only from uncertain regions covering multiple pixels. Based on a qualitative assessment, we tested different sieve sizes. We determined that a minimum size of six pixels provided the best trade-off between maintaining small patches and avoiding sampling isolated pixels.

Once samples for active learning were generated, we identified the crop types and appropriately labelled the samples (Fig. 4). First, we confirmed that the site was indeed farmland by cross-checking with field data, including from UAV and very high resolution satellite images. We then repeated the crop profiling step in 2.2.3 (refer to Fig. 4b). Lastly, to determine the crop type, we examined the crop growth pattern using the PlanetScope monthly NDVI Tropical Mosaics and multispectral images. These steps are demonstrated in Figure 4 using the example of a single pixel in the yam class.

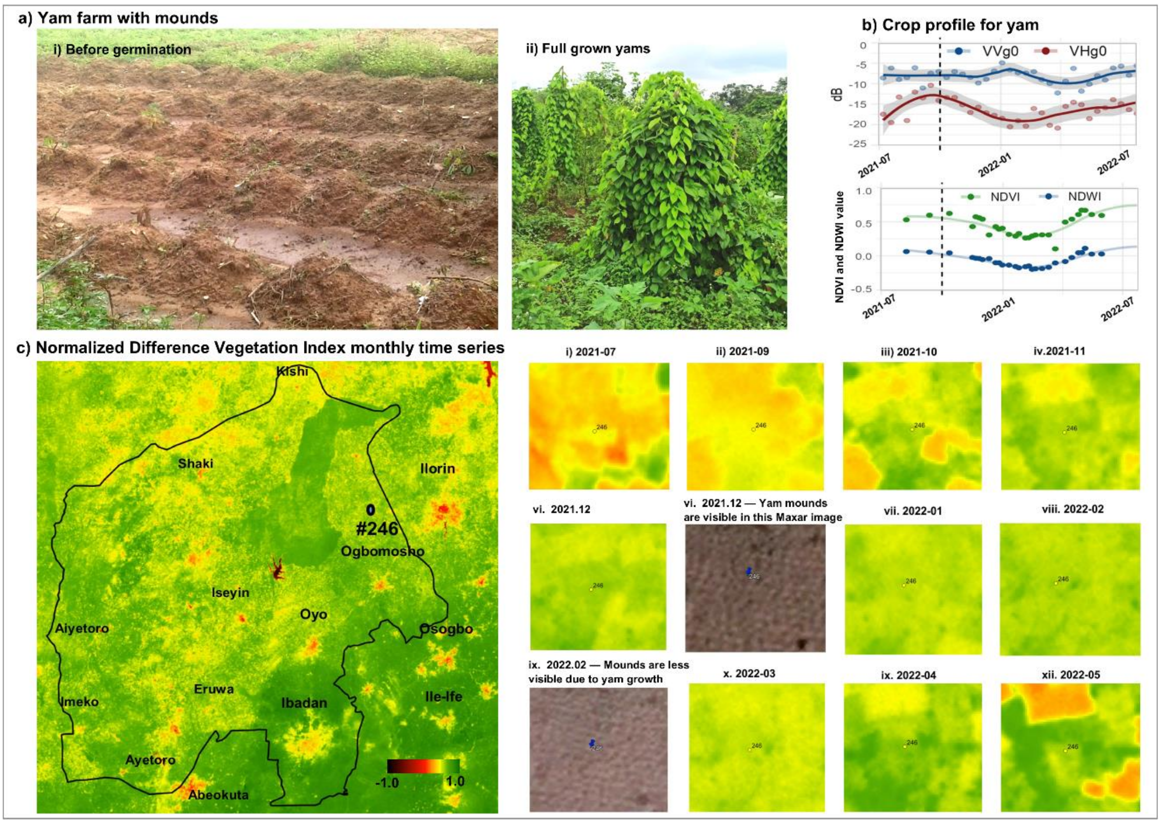

Fig. 4. The procedure used to identify crop types for active learning samples, example of a yam farm (#246), a) The appearance of yam with the mounds varies widely depending on the stage of crop growth (i-ii), b) Crop profile, c) PlanetScope NDVI of May 2022 over the study area, d) Crop growth dynamics of #246 during different phenological stages are depicted in the monthly NDVI time series and very high resolution Maxar images (Google Earth image 2023 Maxar Technologies).

Due to the complex nature of our class catalogue, we identified additional labels for 148 samples in uncertain areas, mainly for the yam and late maize classes. We discarded doubtful samples to avoid introducing other uncertainties to the model. Based on the complemented sets of reference data (n=1,144), we fine-tuned the trained random forest model for prediction and obtained the final map of farming systems in LGS. We based our classification of farming systems on Random Forest models using 250 trees (Breiman et al. 2001) as implemented in Google Earth Engine. This study used a Random forest classifier due to its proven performance in mapping crop types and heterogeneous landscapes. Studies applying random forest classifiers for crop-type mapping in African smallholder contexts include Nigeria (Ibrahim et al., 2021; Abubakar et al., 2023), Mali (Lambert et al., 2018), Kenya (Jin et al., 2019), South Africa (Mazarire et al., 2020). As a nonparametric classifier, Random Forest is considered suitable as the assumption of a normal distributed dataset is relaxed, does not require the use of statistical parameterization for class separation and overcomes the problem of overfitting (Sothe et al., 2017; Ouzemou et al., 2018).

2.2.5 *Cropland masking*

Constraining our farming system classification to cropland pixels required a suitable cropland mask. Therefore, we visually inspected multiple global and continental scale land cover products for their ability to accurately discriminate cropland from non-cropland in our study region. We here considered the 10 m resolution ESRI land cover (ESRI, 2023), ESA WorldCover 2021 (ESA, 2023) and MODIS land cover (Menashe and Friedl, 2018). The timeliness and spatial resolution made these products suitable candidates for cropland masking in LGS. However, most products performed weakly in areas with a high presence of perennial crops with a high share of woody biomass (e.g., yam and cassava with stems of up to 1.5 m).

After careful evaluation, we used the WorldCover to mask out non-croplands from our study region. At 10m spatial resolution, the WorldCover matches our study period relatively well compared to other products available only for earlier years. We combined cropland, grassland and shrubland to avoid the erroneous removal of full-grown cassava and yam fields, especially in the northern parts of our study region.

2.2.6 Validation

We conducted k-fold cross-validation using the reference datasets but excluded the active learning samples. Without wall-to-wall ancillary data that would enable us to generate labels for a random sample, it was not feasible to perform an area-adjusted accuracy assessment (Olofsson et al., 2014). We split our reference data into k=30 groups, iteratively trained Random Forest models with k-1 groups, and then predicted the farming system classes for the held-out sample (n=33). We compared predictions with field data and calculated Overall Accuracy (OA), User Accuracy (UA) and Producer Accuracy (PA) for all eight classes in each fold.

2.3 Field delineation and field size estimation based on deep learning

We further examined whether field size is related to crop type and cropping patterns. We used a deep learning workflow relying on a ResUNet with pre-trained model weights from smallholder farming in India (Wang et al., 2022) and sub-meter imagery in Google Earth Pro™ to delineate individual fields for 2,333 sites distributed across the study region (Fig. 5).

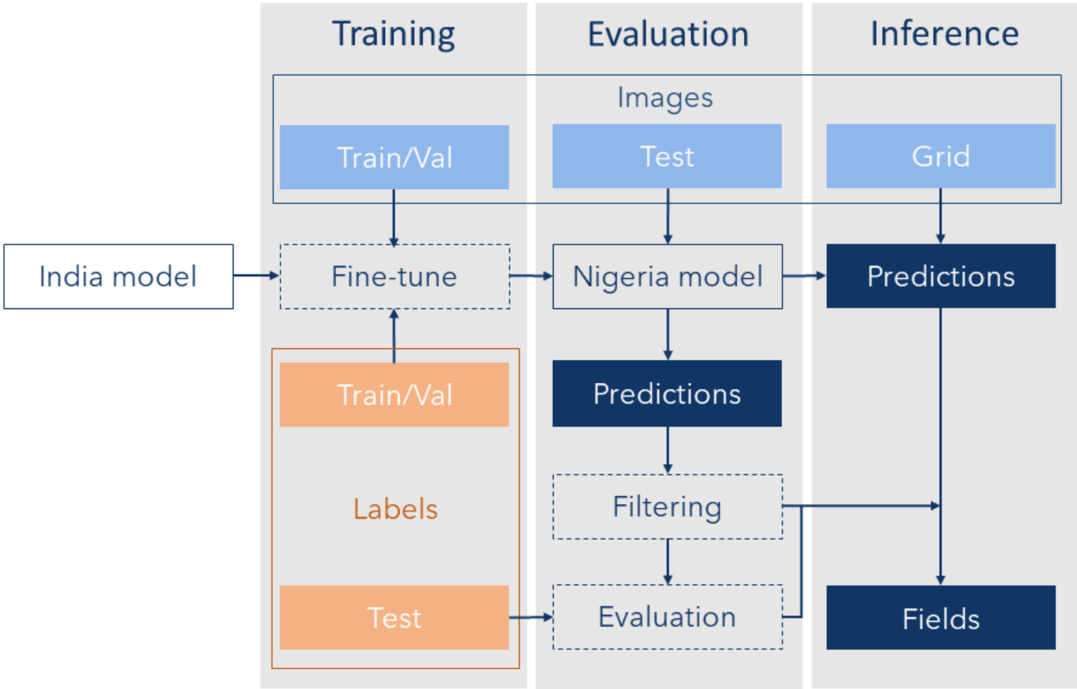

Fig 5. Workflow for field delineation. Val = validation.

2.3.1 Image data and labels

We created a stratified random sample (n = 500) for model training in cropland regions. Using very high resolution images from Google Earth Pro™, we screened individual images for cropland presence and sufficient visibility of field boundaries. We generated a systematic sampling grid with a three km distance to predict field size across the study region. This grid was selected as optimal after evaluation with several grid sizes. We manually digitized all fields for the images meeting these requirements (n = 293), yielding 7,682 polygons representing various field sizes and cropping patterns.

Field sizes in the reference data ranged between 0.01 ha and 59.52 ha (mean of 0.93 ha, standard deviation of 1.69 ha). We divided this digitized field data into training (60%), validation (20%) and test data (20%). We used the polygons to create multi-task labels in raster format representing three layers: 1) a binary layer indicating the presence of a crop field, 2) a binary layer indicating the presence of a field boundary and 3) a continuous layer representing the normalized distance of each field pixel to the nearest field boundary. We removed points with less than 10% cropland in its surrounding area (36 ha), according to the WorldCover 2021 cropland mask. A total of 2,333 sites were returned, which were then used to delineate individual fields and estimate field size at the field, local, and regional levels.

2.3.2 Model training, filtering and evaluation

We used the image data and labels to fine-tune a FracTAL ResUNet, a state-of-the-art model architecture designed to delineate agricultural fields (Waldner et al., 2021). We obtained pre-trained model weights from Wang et al. (2022) and fine-tuned the model for 50 epochs using a batch size of four, a learning rate of 0.0005 and the Adam optimizer (Kingma and Ba 2014).

Our study region's agricultural landscape complexity and diversity challenged the production of accurate field delineations. For some sites, non-cropland patches (e.g., short fallows or clusters of dense shrubs) were falsely detected as a crop field, which can, in the absence of a sufficiently detailed cropland mask, introduce biases in field size estimates. We noted that in these cases, prediction confidence reflected comparatively lower scores. We, therefore, constrained the analyses to fields predicted with high confidence by introducing filtering based on prediction confidence. We first removed incomplete fields in each site because correct field size estimates cannot be obtained from fields extending beyond the predicted image. We then filtered predicted fields (i.e., model delineated fields) based on the prediction confidence, a score derived as the median predicted probability of all pixels within a field being cropland with probabilities of 0 to 1. We conducted sensitivity analyses to obtain the optimal thresholds for filtering field predictions by testing six threshold values between 0.70 and 0.95 in steps of 0.05 (i.e., 0.70, 0.75, 0.80, 0.85, 0.90 and 0.95).

We evaluated the model performance based on predictions of the test split (n = 62 sites) to assess the suitability of the predictions at the field and site levels. We assessed field-level spatial agreement based on mean intersection over union (mean IoU), the fraction of fields with

IoU scores above 0.80 and field-level precision and recall. At the site level, we assessed the agreement in field size estimates using root mean squared error (RMSE), mean absolute error (MAE), and mean error (ME) in hectares and relative mean absolute error (relative MAE), expressing the error in relation to observed field size. We then calculated the weighted mean field size estimates. The weighting of the mean field size estimate accounts for the higher relevance of large fields when calculating the field size at the site level. We conducted sensitivity analyses to identify a good balance between error metrics, high spatial agreement, and site-level field size estimation by evaluating the performance across the six confidence filtering thresholds.

2.3.3 Linking field size and farming systems

We used the predicted samples of the 2,333 sites, removed incomplete field predictions, and filtered based on the confidence threshold obtained from the sensitivity analyses. For the resulting fields, we aggregated our farming system map to the field-level based on the majority class present in each field. Moreover, we estimated the weighted mean field size at the site-level to assess the spatial distribution of field size in the study region. For better interpretation, we categorized field sizes into five classes representing very small (0.00-0.25 ha), small (0.25-0.50 ha), medium (0.50-1.00), large (1.00-2.50 ha), and very large (2.50-10.00 ha) fields.

3. Results

3.1. Mapping heterogeneous farming systems

3.1.1 Accuracy assessment

We assessed the mean overall accuracy and the observed standard deviation in the k-fold cross-validation across all single-sensor and multi-sensor experiments with bimonthly and monthly temporal bins (Table 4). All experiments involving S2 (i.e., experiments 2, 4, 5, 6, 7) yielded overall accuracies above 0.76, whereas experiments involving only S1 (i.e., experiments 1 and 3) did not perform well with overall mean accuracies of 0.50. The highest mean overall accuracy of 0.79 (+/- 0.09) and 0.78 (+/- 0.10) were obtained in experiment 5 (combining monthly S1 and monthly S2 spectral features) and experiment 4 (monthly S2), respectively. However, the maps based on the monthly S2 features alone (i.e., experiments 4 and 5) had a high share of data gaps due to clouds (Fig. 6), which affected 10.2% of the cropland area. Therefore, we decided to base our analyses on the map from experiment 7 (i.e., S1 monthly and S2 bimonthly data), despite the slightly lower mean overall accuracy of 0.77 (+/- 0.08), as it effectively reduced the fraction of data gaps to 0.2%.

Table 4 Overall accuracies across experiments with reported features, mean overall accuracy, standard deviation, and standard error of the mean estimate. Scores were derived from 30-fold cross-validation.

No.	**Experiments**	**mean overall accuracy**	**standard deviation**	**standard error**
1	S1 bimonthly	0.50	0.10	0.02
2	S2 bimonthly	0.76	0.08	0.01
3	S1 monthly	0.50	0.08	0.02
4	S2 monthly	0.78	0.10	0.02
5	S1 monthly + S2 monthly	0.79	0.09	0.02
6	S1 bimonthly + S2 bimonthly	0.76	0.07	0.01
7	S1 monthly + S2 bimonthly	0.77	0.08	0.01

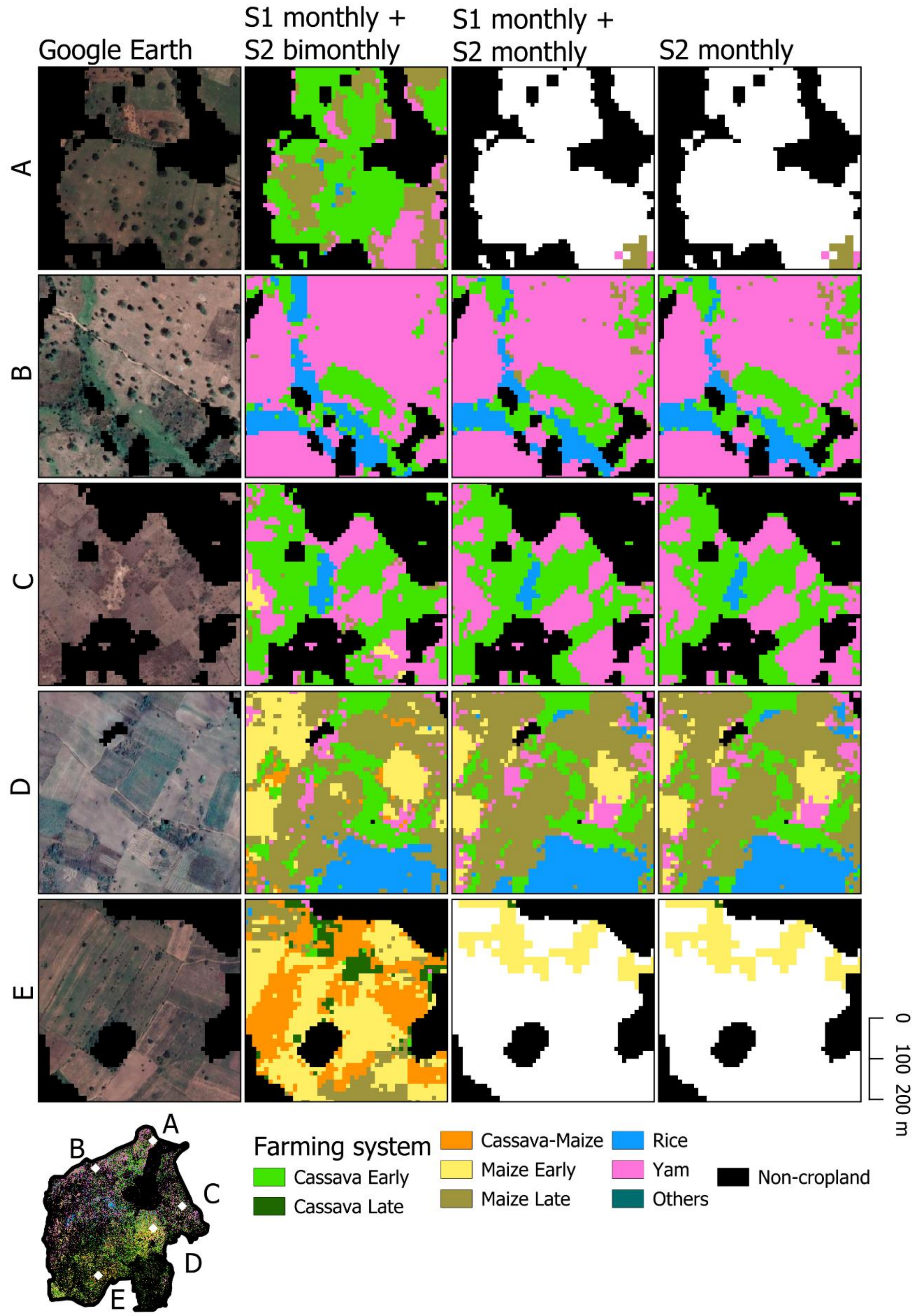

Fig 6: Comparison of Google Earth VHR imagery and three map versions (columns) integrating S1 monthly and S2 bimonthly, S1 and S2 monthly and only S2 at monthly intervals across different parts of the study region (rows). Black pixels indicate non-cropland, and white pixels indicate data gaps, according to WorldCover 2021.

The selected model based on monthly S1 and bimonthly S2 features (experiment 7) yielded high class-specific accuracies, yet with substantial variation across the 30 folds (Fig. 7). Mean user accuracies exceeded 0.70 for all classes, with standard deviations ranging between 0.19 (yam) and 0.32 (Others). The highest mean user accuracies were reached for rice (0.90 +/- 0.18), early maize (0.81 +/- 0.22) and maize-cassava (0.79 +/- 0.20). The lowest user accuracies were for late cassava (0.71 +/- 0.23) and late maize (0.74 +/- 0.27). Mean producer accuracies were particularly high for early maize (0.89 +/- 0.22), maize-cassava (0.85 +/- 0.19), and yam (0.85 +/- 0.19). The lowest mean producer accuracies occurred for late maize (0.58 +/- 0.26) and Others (0.71 +/- 0.31).

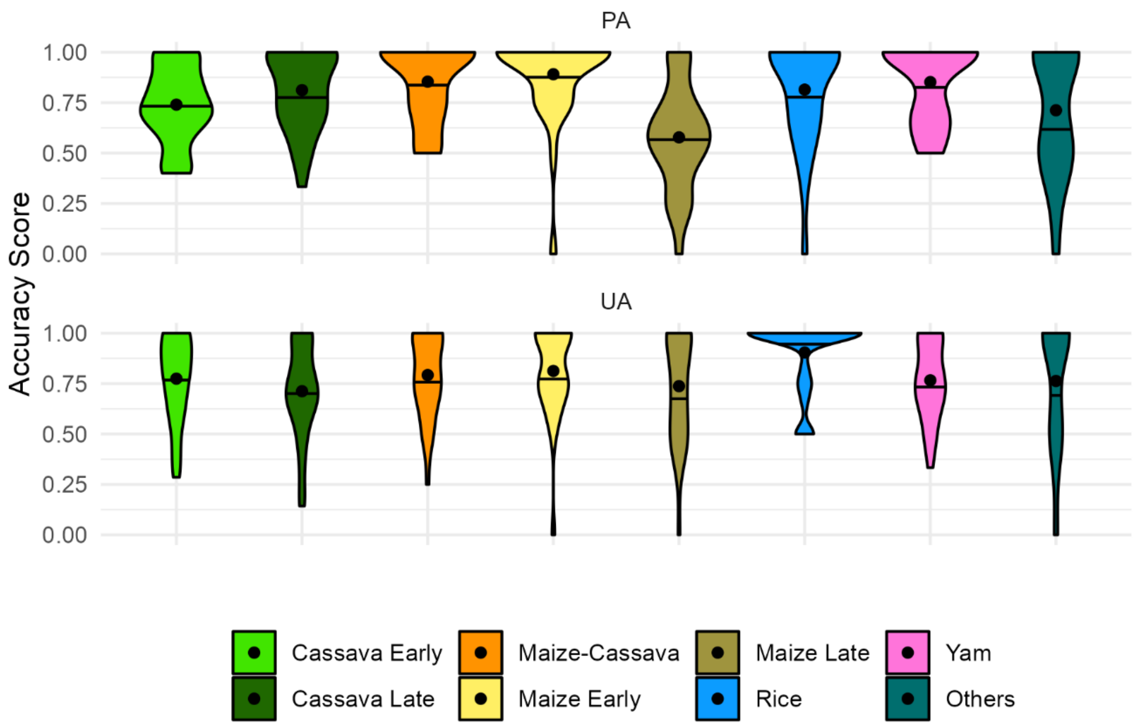

Fig. 7: Class-wise PA (top) and UA (bottom). Scores derived from 30-fold cross-validation. Horizontal lines represent the median score, whereas the points are the mean scores.

3.1.2 Spatial patterns of major farming systems

We mapped the distribution of the eight major farming systems in the LGS. We considered maize, cassava, yam, rice, mixtures of maize-cassava and the Others class (i.e., cocoyam, cowpea and sweet potatoes) during the 2022 early and late planting seasons (Fig. 8).

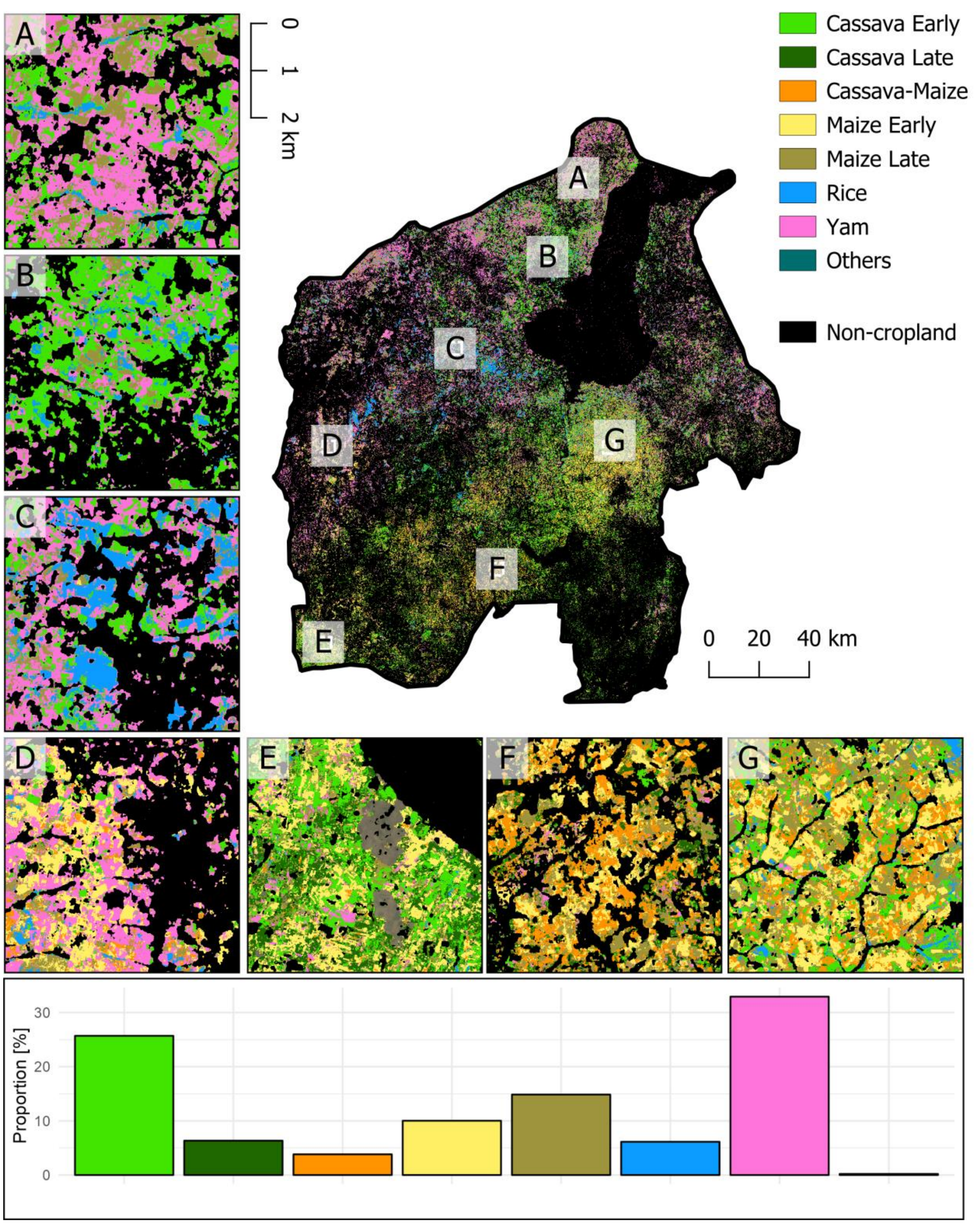

Fig. 8: A-G show close-ups of classification results. A) major yam growing areas near Kishi and Shaki, B) early cassava area near Igboho, C) Lowland rice cultivation in the Igbeti area, D) early and late maize in the Aiyetoro area of Oyo state, E) early and late cassava with early maize near Imeko, F) maize-cassava intercropping in Aborisade near Eruwa, G) late maize and maize-cassava intercropping in the Ogbomosho area (Refer to Fig. 1c for the locations of these settlements). The bar chart depicts the proportion of fields contained in each farming systems.

Although different parts of the LGS specialized in certain crops, yam is widely grown across the region. Overall, the distribution of the farming systems across croplands in the study region was as follows: early cassava: 25.7%, late cassava: 6.3%, maize-cassava: 3.8%, early maize: 10.0%, late maize: 14.9%, rice: 6.1%, yam: 32.9%, and Others: 0.2% (Figure 9)

3.2 Field size analyses

3.2.1 Automated field delineation performance

The evaluation of the field delineation revealed high field-level agreement with mean IoU scores ranging between 0.66 for the 70% and 0.73 for the 95% confidence thresholds (Fig. 9). For all confidence thresholds of 85% and above, at least half of the fields had mean IoU scores of 0.8 or higher. Good balance in precision and recall was achieved at 95% and 85% confidence thresholds, respectively. Field size estimates at the site level had the lowest RMSE (0.983 ha) and MAE (0.603 ha) when using 75% confidence thresholds. However, ME (i.e., bias) was lowest (0.023 ha) at 85% (46.5%), whereas MAE at 75% was 40.8%. Due to the high level of spatial agreement and the overall low bias in field size estimates, we decided to use the 85% confidence threshold for filtering the predictions across the sample grid.

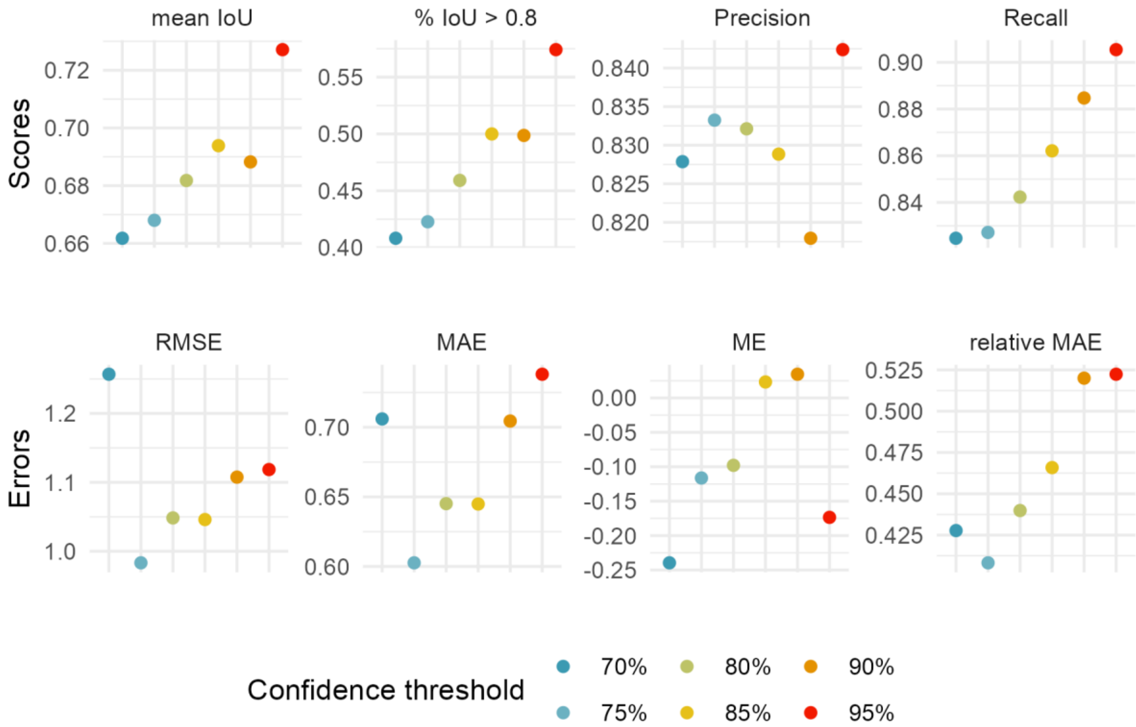

Fig. 9: Evaluation of field-level spatial agreement (top row) and site-level field size estimation (bottom row) based on test split (n sites =62) across confidence thresholds used for filtering.

3.2.2 Field size distribution

We assess the distribution of mean field sizes across the study region based on the sample grid at three km distance (Fig. 10). With a mean field size of 0.6 ha, we observed a dominance of medium field sizes (0.50-1.00 ha), which clustered across large parts of the study region. Both medium and large (1.00 - 2.50 ha) field sizes were prevalent at the site level, while very large (2.50 - 10.00 ha) field sizes were scattered and comparatively rare. Very small (< 0.25 ha) and small (0.25 - 0.50 ha) fields were mainly found in the more fragmented landscapes in the southeastern and western parts of the study region, where the share of agricultural land is comparatively low and natural vegetation persists. Differences in field sizes ranged from larger fields in the North, where yam and cassava are predominantly grown, to smaller fields in the southern region. Larger monocropping fields, especially for yam, were more in the northern part of our study area, whereas much smaller and heterogenous fields to the South. The southeastern parts include the urban environment around Ibadan, which is transitioning into the rainforest ecosystem and is thus dominated by forests. The western and northern section of the study region is characterized by savanna vegetation.

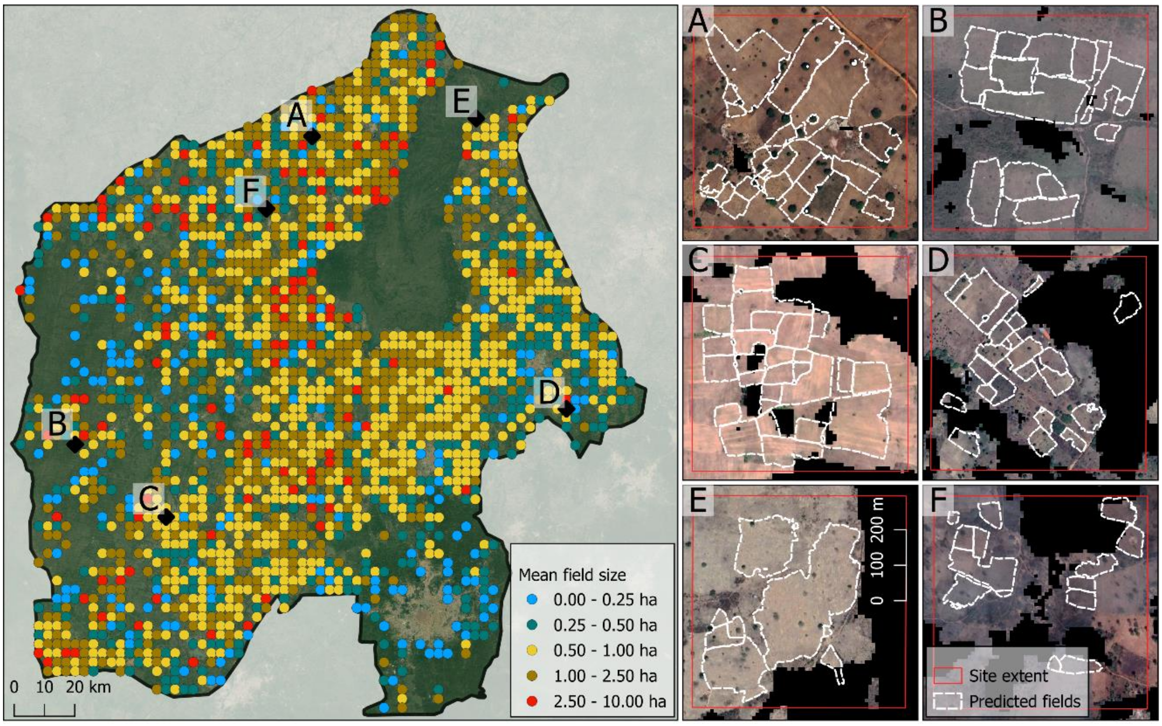

Fig. 10: Spatial distribution of mean field size (left) and examples of field predictions filtered using the 85% confidence threshold (A-F).

3.2.3 Relating field sizes to farming systems

We intersected the model-delineated fields with the farming system map to explore field size distribution across the different farming systems. Filtering the model-delineated fields in all 2,333 sites using the 85% confidence threshold resulted in 14,000 fields with a size ranging between 0.001 ha and 9.9 ha. We then intersected this field size output with our farming system map and assigned the majority farming system to each model-delineated field.

Relating field size to farming systems, the region was dominated by small fields (52.2%) and medium-sized fields (25.1%), followed by large (13.2%), very small (7.4%), and very large fields (2.2%). On average, the mean field size was 0.6 ha. Stratifying across farming system classes, medium to larger fields (>0.5 ha) were more frequent for early cassava, late maize and rice (Fig. 11a). A stratification of farming systems and field size revealed a similar distribution of field size categories across the farming systems (Fig 11b).

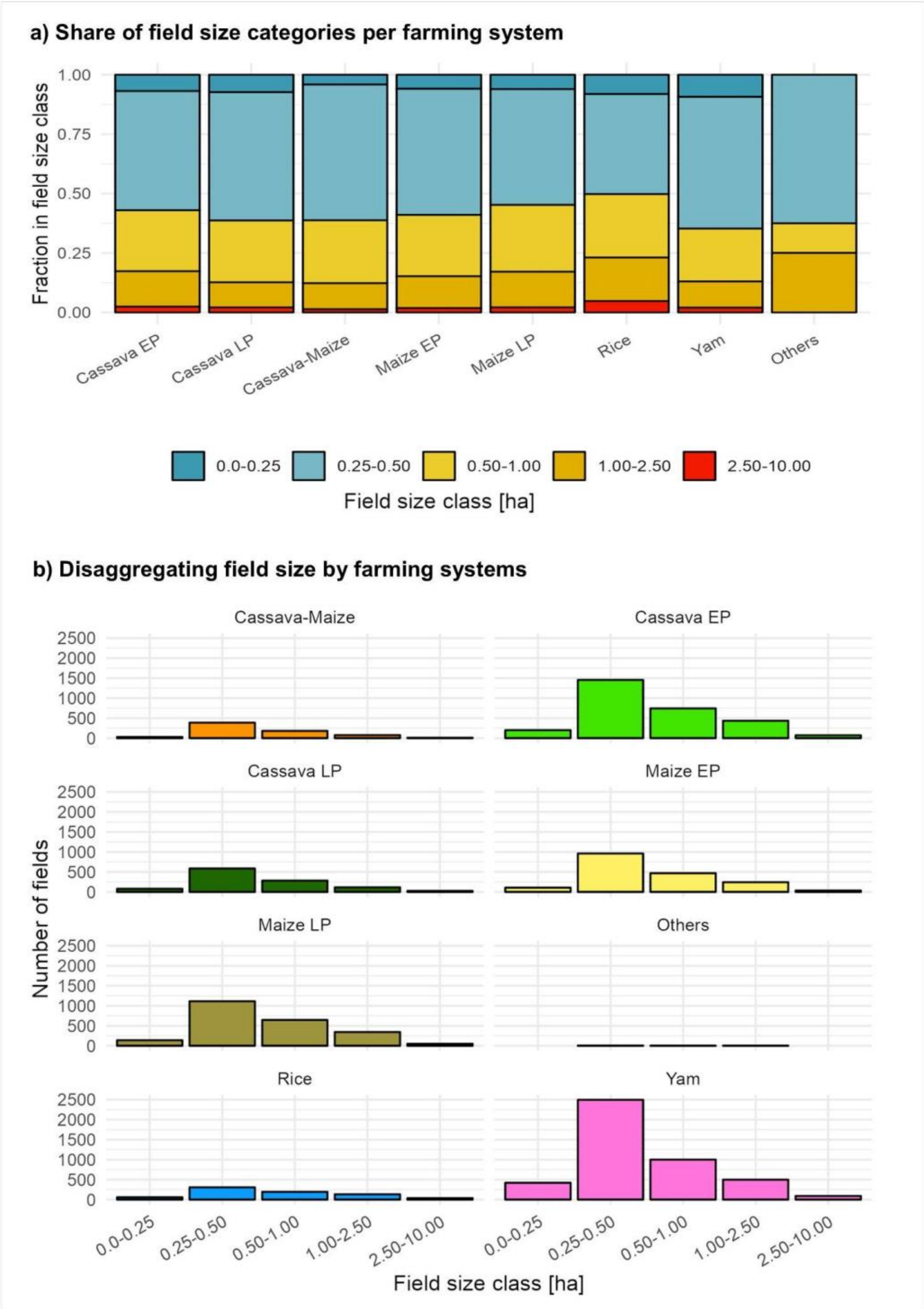

Figure 11 Relating field size categories to farming systems. a) Relative share of field size class per farming system, b) Histograms relating field size categories to farming systems

Maize-cassava and late cassava showed lower shares of large and very fields. The number of fields present for each farming system reflects the overall proportions of the mapped farming systems. As such, only a few fields of the Others class were included in this analysis. Fields below 0.25 ha were comparatively rare in the study region, but fields of 0.25 - 0.50 ha dominated all farming systems.

4 Discussion

4.1 Spectral-temporal metrics from Sentinel 1 and Sentinel 2

The smallholder agricultural settings we studied fall within the lower Guinea Savannah of southwest Nigeria. As in many parts of the tropics, the region is characterized by incessant cloud cover. Clouds and associated shadows critically challenge the use of optical sensors (Whitcraft et al., 2015; Danso et al., 2019). Hence, the temporal frequency of usable S2 images, especially during the growing seasons, is drastically reduced. This necessitated using S1 radar data whose observations do not depend on solar illumination or atmospheric conditions (Khabbazan et al. 2019) in combination with S2, providing richer spectral information.

Our experiments returned lower overall accuracies of about 0.50 when only S1 features were used. Some studies (e.g., Kpienbaareh et al., 2021; Rao et al., 2021) confirm the inadequacy of S1 data for crop type mapping in smallholder contexts despite reports of better results in the range of 0.85 - 0.90 in other agricultural contexts and regions (e.g., Veloso et al., 2017; Vreugdenhil et al., 2018; Khabbazan et al., 2019; Planque et al. 2021). Veloso et al. (2017) demonstrated that S1 (particularly the VH/VV ratio) yielded valuable information on crop development after comparing fresh biomass, NDVI, precipitation and temperature to S1 data. They noted the potential to distinguish between crops based on the temporal variation of backscatter, especially for barley and maize. Similarly, Planque et al. (2021) reported that S1 backscatter and interferometry show a high consistency for crop monitoring and detecting key dates for important crops in the Netherlands. They highlighted that structural and biomass changes associated with crop development influenced the backscatter for each crop class mapped throughout the season. These examples of achievements using S1 mainly relate to monocropping systems in developed countries, which are less complex than our smallholder setting.

Further, our results improved to 0.78 using only S2, especially the monthly S2 features, despite cloud cover and related artefacts. This better result with S2 is in line with most studies on smallholder agriculture in Africa using only S2 for crop type mapping, such as in Nigeria (Ibrahim et al., 2021), Mali (Lambert et al., 2018), Kenya (Jin et al., 2019), and South Africa (Mazarire et al., 2020). However, the use of S2 features alone was precluded for our study region because of the lack of data in about 10% of the area studied. The non-availability of S2 data within the critical temporal windows in the growing season is a limitation for crop type mapping in smallholder regions such as ours. The availability of cloud-free optical (S2) observations was essential in differentiating crop phenology and, ultimately, crop types (Frantz, 2019), especially within the identified critical temporal windows for crop type differentiation and mapping (Griffiths et al., 2019; Ibrahim et al., 2021). Ibrahim et al. (2021) reported the importance of S2 spectral bands performing well when systematic narrow temporal critical windows are used in predicting intercropped classes.

4.2 Mapping of multiple crops and intercropping

Most remote sensing studies do not account for intercropping and multiple growing cycles in classifying and predicting crop types (Jin et al., 2019; Ibrahim et al., 2021). To improve the identification of multiple crops, especially crops growing in intercropping systems, we screened our sample data (both field-based and from satellite imagery) for quality. The 3m PlanetScope images (i.e., multispectral and monthly NDVI) and 0.6m resolution Maxar images were most helpful in confirming crop growth patterns in the crop profiles created with S1 and S2. Crop types were identified based on crop phenology from satellite imagery, geotagged pictures, and RGB imagery from UAV. Samples were discarded in areas where very high-resolution images were unavailable for the required date. We recommend better access to higher resolution images to meet the challenges of mapping the heterogeneous agricultural landscapes typical of smallholder farms. This decade (2019–2028) is the Decade of Family Farming (United Nations, 2017), which is typical of most smallholder farms. However, not all smallholder farms are family farms (Lowder et al., 2021).

A novelty we present in this section is harnessing the monthly NDVI time series to visually identify spatio-temporal phenology stages to actively label different crop types, which can be applied in similar smallholder regions. Temporal characteristics of farming activities – field clearing, crop emergence, crop peaking and senescence stages – helped to identify and label different crop types, especially for the early and late planted maize classes, for which their growth stages in the early or late part of the growing season was most critical for identification. We considered it essential to capture intercropping as it is the dominant farming practice in smallholder farming systems, especially in Africa. Perception studies among smallholder farmers have found that farmers intercrop to forestall total crop failure. For example, drought is perceived to impact crops differently. Likewise, intercropping provides nutritional options, enables nitrogen fixation by legumes, and sometimes serves as a physical barrier to pests and diseases (Bouws and Finckh, 2008; Akinyemi, 2017; Kinyua et al., 2023).

From a remote sensing methods point-of-view, identifying and predicting crops in intercropping systems (e.g., maize-cassava) is particularly challenging because of the different sowing dates, similarity in the crops' comparable height and structure. Yam was the easiest to detect in our study region from very high resolution images due to its distinct ridges or mound patterns. However, full-grown yams are often spectrally similar to tree crops and shrubs in smallholder farms. We found that yam occupied about 40% of the land area in our study region. The cassava class also exhibited a slight distinction in texture from the Others class. As cassava can grow more than 1.5m, it was difficult to distinguish it from tree crops and shrubs. The maize class was challenging to identify or improve using the active learning methodology, as it revealed no distinct pattern and texture across all growing stages. The rice class was identified well by its smooth texture and being associated with floodplains. Using field-based information about cropping patterns and crop management practices (e.g., crop sowing dates and sequence), we could label samples for all classes except mixtures using our active learning methodology. Identified crop mixture samples such as intercropping from very high resolution images were discarded as these were particularly doubtful considering the mixed crop signatures in the images and different growth stages of the crops. The overall pattern of monocropping fields of early cassava, late maize, rice and yam clustered mostly in the North, whereas intercropped fields of maize-cassava and monocropped late maize were mainly present in the fragmented agricultural landscapes in the South.

From an economic perspective, the study focused on identifying major farming systems for producing major food staples that are widely consumed locally to ensure their relevance in meeting the domestic food needs of the region and to infer feasible surpluses for export. For example, cassava is an economic crop that is processed locally into different food products. Cassava is equally important for local industry and export, e.g., for producing ethanol and cassava chips for battery production (Kolawole et al., 2010; Srivastava et al., 2023). Maize and cassava are two crops favoured for intercropping by farmers for economic reasons (Nwokoro et al., 2021; Kinyua et al., 2023). While cassava matures after 12 months, maize is fast growing and ready for harvest in 2.5 - 3 months – a so-called “hunger-combating crop”. Moreover, farmers in this and similar smallholder regions take advantage of the multiple growing cycles in the region to grow crops several times a year.

4.3 Relating field size to cropping systems

We established the empirical relationship between field size and cropping systems in the smallholder farming systems of LGS. The first step was to detect individual fields at very high spatial resolution with Deep Transfer Learning and then to intersect delimited fields from the model with the farming system map. Deep learning segmentation of field size using automation algorithms is becoming an efficient tool for delineating field sizes (Waldner et al., 2020). However, these methods are challenged in smallholder regions with heterogeneous farming systems, often changing field borders or having no clear field borders (Samberg et al., 2016; Fatunbi et al., 2020). Irregular crop field patterns and sometimes drainage channels created within a farm complicate deciding where the boundary of one farm ends without very clear field demarcations or cadastre information. Despite these challenges in smallholder systems, Wang et al. (2022) demonstrated the robustness of the methodology we adopted for Indian smallholder settings. Similarly, we achieved high accuracy in extracting field outlines and deriving field size information.

Monocropping was positively related to larger field sizes in the LGS. From a historical perspective, Nigeria has pursued agricultural land expansion programmes requiring land to be converted to croplands, resulting in extensive forest clearing for agricultural purposes (Ekong, 1983; Akinyemi, 2013; Akinyemi and Ifejika Speranza, 2022). Associated with the expansion of croplands was the structural change to smallholder agriculture, from a highly subsistence structure to commercial, which is reflected in changing field sizes. The spatial distribution of field size across the region reveals a mean field size of 0.60 ha with variations between different farming systems. Although the share of field size was dominated by small fields (52%) and medium-sized fields (25%), large to very large fields covered 15.4% of our study region. We question whether smallholder crop fields are still to be generalized at sizes of <2 to 5 ha for sub-Saharan Africa (FAO, 2015; Banerjee et al., 2015; Fritz et al., 2019). In our analysis of field sizes, some fields were found within >1.0 to 10 ha thresholds. These thresholds are larger than the *very small* (<0.64 ha) and *small field* (0.64 - 2.56 ha) classifications where the majority (87%) of Nigeria's fields were captured, according to Lesiv et al. (2019). The occurrence of larger field sizes in our study region can be attributed to the emergence of *step-up farmers,* i.e., smallholder farmers who expanded their farming operations from small to medium-sized fields and the influx of *step-in* farmers, i.e., diaspora investments in the agricultural sector associated with increasing agri-businesses (Chiaka et al., 2022). Chiaka et al. (2022) found a proportional increase in medium- and large-sized farms in Nigeria between 2015 and 2018. Jayne et al. (2022) found an increasing trend in the rise of medium-sized farms in seven African countries. They attributed the increase in field size to investor farmers and the policy efforts supporting agricultural transformation in Africa.

5. Conclusions

To our knowledge, a few examples demonstrate the opportunities of satellite remote sensing for mapping multiple crops and intercropping across multiple growing cycles. These are the critical gaps this study fills using as a case the complex and heterogeneous smallholder systems of the lower Guinea Savannah of Nigeria. Like most parts of sub-Saharan Africa, Nigeria lacks crop type maps even though they are baseline data for food security and planning. With the mapping complexities associated with smallholder agriculture, our results revealed the potential of combining optical and radar (e.g., S2 and S1) data. Better crop type prediction in heterogeneous farming systems, including intercropping and dual cropping cycles, was achieved, which was previously lacking in the literature. Different combinations of monthly and bimonthly S1 and S2 features achieved accuracies ranging from 76 to 79%, which are comparable to most monocropping and single cropping cycle studies. Like most previous studies, our findings suggest improving the mapping accuracy with the combination of multiple sensors. Integrating the new Environmental Mapping and Analysis Program (EnMap) hyperspectral bands with S1 and S2 images may improve crop type mapping in smallholder agriculture despite mapping challenges. For example, the narrower spectral windows of the EnMap may provide critical spectral information for capturing crop mixtures in heterogeneous smallholder regions as they are currently not explored to our knowledge.

Our approach allowed us to define eight farming system classes indicating crop types, crop mixtures, and the planting period during the first planting season (i.e., early growing cycle) and the second (late growing cycle). We perceive room for improvement by separating crops combined in the Others class containing multiple crop types such as cocoyam, cowpea and sweet potato. As there might be omission errors in the Others class, separating crops in this class may provide a more robust outlook. We had spectral mixtures between yam and cassava with shrubs and tree crops, whether in mono- or intercropping farming systems. Consequently, this study did not consider tree crops to minimize the complexity of mapping mixed farming systems with Remote Sensing, especially when developing each crop's phenology and experimenting with combinations of S1 and S2 features. We now recommend explicit methodology for separating tree crops and perennial crops (e.g., yam and cassava) in future studies.

By mapping multiple crops and differentiating cropping patterns into mono- and intercropping using Remote Sensing and Machine Learning, the information provided in this study is valuable for future downstream assessments of crop production and yields and the inference of the influence of agricultural structural changes such as farm consolidation on crop production. We recommend adapting our methodology to produce wall-to-wall crop type maps for similar regions.

Acknowledgements

This research was conducted within the Land-use Change and the Resilience of Food Production Systems (LucFRes) project. This project has received funding from the European Union (EU) Horizon 2020 research and innovation programme under the Marie Skłodowska-Curie (grant agreement no. 101025259). The Women in Natural Sciences Award granted to Dr. Akinyemi by the Einstein Foundation and the Berlin University Alliance in 2023 is also gratefully acknowledged. Dr. Rufin was supported by the Fund for Scientific Research – Fonds de la Recherche Scientifique (grant agreement no. T.0154.21). We would like to thank the Agricultural Development Programme officials of the Ministry of Agriculture, Commodity farmers' associations, the communities visited, farmers for their time and for sharing valuable farm management practices, and the various local fieldwork team members whose names are too numerous to mention. We are also grateful for access to PlanetScope scenes and Tropical Mosaic images by Planet-NICFI and Planet's Education and Research Program. We appreciate the free and open access to Sentinel-1 and Sentinel-2 data and open cloud geospatial processing tools in Google Earth Engine. This study contributes to the Global Land Programme (https://glp.earth) and the Programme on Ecosystem Change and Society (https://www.pecs-science.org). All content and information contained in this article reflect only the authors' views and not that of the EU, the European Union Horizon 2020 or any other body.

Software

All images were processed in Google Earth Engine.

CRediT authorship contribution statement

Felicia O. Akinyemi: Conceptualization, Survey design and reference data collection, Methodology, Formal analysis, Visualization, Writing – original draft, Writing – review & editing, Funding acquisition. **Philippe Rufin**: Conceptualization, Methodology, Formal analysis, Software, Visualization, Writing – original draft, Writing – review & editing. **Esther Shupel Ibrahim**: Methodology, Writing – review & editing. **Patrick Hostert**: Methodology, Writing – review & editing. **Lucia O. Ogunsumi**: Cropping calendar and survey design, Agricultural Development Programme and Extension services. **Olugbenga A. Egbetokun**: Cropping calendar, Farmers' Survey. **Chinwe Ifejika Speranza:** Conceptualization, Writing – review & editing, Supervision, Funding acquisition.

Declaration of Competing Interest

The authors declare that they have no known competing financial interests or personal relationships, and neither has any funder influenced the work reported in this paper at any stage from design to submission.

Data availability

Sources of all datasets used are specified in the manuscript. Data are made available in Zenodo after acceptance.

References

Abubakar, G.A., Wang, K., Koko, A.F., Husseini, M.I., Shuka, K.A.M., Deng, J., Gan, M. (2023). Mapping maize cropland and land cover in semi-arid region in northern Nigeria using Machine Learning and Google Earth Engine. Remote Sensing 15(11):2835. https://doi.org/10.3390/rs15112835

Akinyemi, F.O. (2013). An assessment of land use change in the cocoa belt of south west Nigeria. International Journal of Remote Sensing, 34(8): 2858-2875. https://doi.org/10.1080/01431161.2012.753167

Akinyemi, F.O. (2017). Climate change and variability in semi-arid Palapye, Eastern Botswana: An assessment from smallholder farmers' perspective. Weather Clim. Soc., 9:349-65. https://doi.org/10.1175/WCAS-D-16-0040.1

Akinyemi, F.O., Ifejika Speranza, C. (2022). Agricultural landscape change impact on the quality of land: An African continent-wide assessment in gained and displaced agricultural lands. International Journal of Applied Earth Observations and Geoinformation, 106:102644. https://doi.org/10.1016/j.jag.2021.102644

Ayoola, O.T., Makinde, E.A. (2007). Fertilizer treatment effects on performance of cassava under two planting patterns in a cassava-based cropping system in South West Nigeria. Res. J. Agric. Biol. Sci., 3 (1), 13–20.

Becker-Reshef, I., Barker, B., Whitcraft, A., Oliva, P., Mobley, K., Justice C., Sahajpal, R. (2023). Crop type maps for operational global agricultural monitoring. Scientific Data, 10, 172. https://doi.org/10.1038/s41597-023-02047-9

Bizikova, L., De Brauw, A., Rose, M.E., Laborde, D., Motsumi, K., Murphy, M., Parent, M., Picard, F., Smaller, C. (2022). Achieving sustainable food systems in a global crisis: Nigeria country roadmap to end hunger, double farmer incomes, improve diets, and protect the climate. International Institute for Sustainable Development. https://www.iisd.org/system/files/2022-09/sustainable-food-systems-global-crisis-nigeria.pdf [accessed 15 Nov. 2023].

Bouws, H., Finckh, M.R. (2008). Effects of strip intercropping of potatoes with non-hosts on late blight severity and tuber yield in organic production. Plant Path 57, 916–927.

Breiman, L. (2001). Random forests. Machine Learning, 45:5-32. https://doi.org/10.1023/A:1010933404324

Banerjee, R., Carletto, C., Jolliffe, D.M. (2015). From tragedy to renaissance: Improving agricultural data for better policies. Policy research working paper no. WPS 7150, LSMS, Washington, D.C.: World Bank. http://documents.worldbank.org/curated/en/313131468194048389/From-tragedy-to-renaissance-improving-agricultural-data-for-better-policies [Accessed 15 Nov. 2023]

Chiaka, J.C., Zhen, L., Yunfeng, H., Xiao, Y., Muhirwa, F., Lang, T. (2022). Smallholder farmers contribution to food production in Nigeria. Front. Nutr. 9:916678. https://doi.org/10.3389/fnut.2022.916678

Danso, D.K., Anquetin, S., Diedhiou, A., Lavaysse, C., Kobea, A., Touré, N.D.E. (2019). Spatio-temporal variability of cloud cover types in West Africa with satellite-based and reanalysis data. Quarterly Journal of the Royal Meteorological Society, 145(725): 3715-3731.

Ekong, E.E. (1983). Farm size, agricultural and rural development in Nigeria. Agricultural Administration, 14(3): 169-183. https://doi.org/10.1016/0309-586X(83)90014-6

Famine Early Warning System Network (2023a). Nigeria Food Security Outlook, June 2023 - January 2024. FEWS NET. https://reliefweb.int/report/nigeria/nigeria-food-security-outlook-june-2023-january-2024 [Accessed 01 Dec. 2023].

Famine Early Warning System Network (2023b). Nigeria Food Security Outlook, October 2023 - May 2024. FEWS NET. https://reliefweb.int/report/nigeria/nigeria-food-security-outlook-october-2023-may-2024 [Accessed 01 Dec. 2023].

FAO (2014). The state of food and agriculture 2014: Innovation in family farming food and agriculture organization of the United Nations. https://policycommons.net/artifacts/2071892/the-state-of-food-and-agriculture-sofa-2014/2827191/ [Accessed 01 Dec. 2023].

FAO (2016). The state of food and agriculture: Climate change, agriculture and food security. FAO, Rome. https://www.fao.org/3/i6030e/I6030E.pdf [Accessed 01 Dec. 2023].

Fatunbi, A.O., Ajayi, M.T., Akinbamijo, O.O. (2020). Strategies for transforming smallholder farming in Africa. Forum for Agricultural Research in Africa (FARA), Accra Ghana, pp. 1-121 Available online at https://library.faraafrica.org/mp-files/strategies-for-transforming-smallholder-farming-in-africa-ofatunbi.pdf [accessed 2023 May 27]

Fritz, S., See, L., Bayas, J.C.L., Waldner, F., Jacques, D., Becker-Reshef, I., Whitcraft, A., Baruth, B., Bonifacio, R., Crutchfield, J., Rembold, F., Rojas, O., Schucknecht, A., Van der Velde, M., Verdin, J., Wu, B., Yan, N., You, L., Gilliams, S., Mücher, S., Tetrault, R., Moorthy, I., McCallum, I. (2019). A comparison of global agricultural monitoring systems and current gaps. Agricultural Systems, 168, 258-272. https://doi.org/10.1016/j.agsy.2018.05.010.

Gorelick, N., Hancher, M., Dixon, M., Ilyushchenko, S., Thau, D., & Moore, R. (2017). Google Earth Engine: Planetary-scale geospatial analysis for everyone. Remote Sensing of Environment, 202:18-27. https://doi.org/10.1016/j.rse.2017.06.031

Griffiths, P., Nendel, C., Hostert, P. (2019). Intra-annual reflectance composites from Sentinel-2 and Landsat for national-scale crop and land cover mapping. Remote Sens. Environ., 220, 135–151.

Ibrahim, E.S., Rufin, R., Nill, L., Kamali, B., Nendel, C., Hostert, P. (2021). Mapping crop types and cropping systems in Nigeria with Sentinel-2 imagery. Remote Sensing 13(17), 3523. https://doi.org/10.3390/rs13173523

Iloeje, N.P. (2001). A new geography of Nigeria (new revised edition). Longman Nig. Ltd: Lagos, Nigeria, p.200.

Jayne, T.S., Wineman, A., Chamberlin, J., Muyanga, M., Yeboah, F.K. (2022). Changing farm size distributions and agricultural transformation in Sub-Saharan Africa. Annu. Rev. Resour. Econ. 14, 109–130. https://doi.org/10.1146/annurev-resource-111220-025657

Jin, Z., Azzari, G., You, C., Di Tommaso, S., Aston, S., Burke, M., Lobell, D.B. (2019). Smallholder maize area and yield mapping at national scales with Google Earth Engine. Remote Sensing of Environment 228, 115-128. https://doi.org/10.1016/j.rse.2019.04.016

Johnson, D.J. (2014). An assessment of pre- and within-season remotely sensed variables for forecasting corn and soybean yields in the United States. Remote Sensing of Environment, 141, 116-128. https://doi.org/10.1016/j.rse.2013.10.027

Karlson, M., Ostwald, M., Bayala, J., Bazié, H.R., Ouedraogo, A.S., Soro, B., Sanou, J., Reese, H. (2020). The potential of Sentinel-2 for crop production estimation in a smallholder agroforestry landscape, Burkina Faso. Front. Environ. Sci. 8. https://doi.org/10.3389/fenvs.2020.00085

Khabbazan, S., Vermunt, P., Steele-Dunne, S., Ratering Arntz, L., Marinetti, C., van der Valk, D., Iannini, L., Molijn, R., Westerdijk, K., van der Sande, C. (2019). Crop monitoring using Sentinel-1 data: A case study from The Netherlands. Remote Sensing, 11(16): 1887. https://doi.org/10.3390/rs11161887

Kingma, D.P., Ba, J. (2017). Adam: A method for stochastic optimization. 3rd International Conference for Learning Representations, San Diego. https://doi.org/10.48550/arXiv.1412.6980

Kinyua, M.W., Kihara, J., Bekunda, M., Bolo, P., Mairura, F.S., Fischer, G., Mucheru-Muna, M.W. (2023). Agronomic and economic performance of legume-legume and cereal-legume intercropping systems in Northern Tanzania. Agricultural Systems 205, 103589. https://doi.org/10.1016/j.agsy.2022.103589.

Kolawole, P.O., Agbetoye, L., Ogunlowo, S.A. (2010). Sustaining world food security with improved cassava processing technology: The Nigeria experience. Sustainability 2, 3681–3694.

Kpienbaareh, D., Sunm X., Wang, J., Luginaah, I., Bezner, K.R., Lupafya, E., Dakishoni, L. (2021). Crop type and land cover mapping in northern Malawi using the integration of Sentinel-1, Sentinel-2, and PlanetScope satellite data. Remote Sensing, 13(4):700. https://doi.org/10.3390/rs13040700

Lambert, M.-J., Traoré, P.C.S., Blaes, X., Baret, P., Defourny, P. (2018). Estimating smallholder crops production at village level from Sentinel-2 time series in Mali's cotton belt. Remote Sensing of Environment, 216, 647–657. https://doi.org/10.1016/j.rse.2018.06.036

Lesiv, M., Laso Bayas, J.C., See, L., Duerauer, M., Dahlia, D., Durando, N., Hazarika, R., Kumar Sahariah, P., Vakolyuk, M., Blyshchyk, V. (2019). Estimating the global distribution of field size using crowdsourcing. Glob. Chang. Biol. 25 (1), 174-186. https://doi.org/10.1111/gcb.14492

Lowder, S.K., Sánchez, M.V., Bertini, R. (2021). Which farms feed the world and has farmland become more concentrated? World Development, 142, 105455. https://doi.org/10.1016/j.worlddev.2021.105455

Mazarire, T.T., Ratshiedana, P.E., Nyamugama, A., Adam, E., Chirima, G. (2020). Exploring machine learning algorithms for mapping crop types in a heterogeneous agriculture landscape using Sentinel-2 data. A case study of Free State Province, South Africa. South African Journal of Geomatics 9(2):333-347. https://doi.org/10.4314/sajg.v9i2.22

Menashe, D., Friedl, M.A. (2018). User Guide to Collection 6 MODIS Land Cover (MCD12Q1 and MCD12C1) Product Sulla- https://lpdaac.usgs.gov/documents/101/MCD12_User_Guide_V6.pdf [Accessed 01 Dec. 2023]

Ministry of Agriculture and Natural Resources (1959). Future Policy of the Ministry of Agriculture and Natural Resources. Ibadan: Government Printer, p. 12.

Muyanga, M., Aromolaran, A., Jayne, T., Liverpool-Tasie, S., Awokuse, T., Adelaja, A. (2019). Changing farm structure and agricultural commercialisation in Nigeria. Agricultural Policy Research Policy in Africa working paper 26, Future Agricultures Consortium. https://opendocs.ids.ac.uk/opendocs/handle/20.500.12413/16699

Nwokoro, C.C., Kreye, C., Necpalova, M., Adeyemi, O., Busari, M., Tariku, M., Tokula, M., Olowokere, F., Pypers, P., Hauser, S., Six, J. (2021). Developing recommendations for increased productivity in cassava-maize intercropping systems in Southern Nigeria. Field Crops Research 272,108283. https://doi.org/10.1016/j.fcr.2021.108283

Olasantan, F.O., Ezumah, H.C., Lucas, E.O. (1996). Effects of intercropping with maize on the micro-environment, growth and yield of cassava. Agric. Ecosyst. Environ. 57 (2),149–158. https://doi.org/10.1016/0167-8809(96)01019-5

Olofsson, P., Foody, G.M., Herold, M., Stehman, S.V., Woodcock, C.E., Wulder, M.A. (2014). Good practices for estimating area and assessing accuracy of land change. Remote Sensing of Environment 148, 42-57. https://doi.org/10.1016/j.rse.2014.02.015.

Omotilewa, O.J., Jayne, T.S., Muyanga, M., Aromolaran, A.B., Liverpool-Tasie, L.S.O., Awokuse, T. (2021). A revisit of farm size and productivity: Empirical evidence from a wide range of farm sizes in Nigeria. World Development 146, 105592. https://doi.org/10.1016/j.worlddev.2021.105592

Ouzemou, J.-E., El Harti, A., Lhissou, R., El Moujahid, A., Bouch, N., El Ouazzani, R., Bachaoui, E.M., El Ghmari, A. (2018). Crop type mapping from pansharpened Landsat

8 NDVI data: A case of a highly fragmented and intensive agricultural system. Remote Sensing Applications: Society and Environment, 11, 94-103.

Planque, C., Lucas, R., Punalekar, S., Chognard, S., Hurford, C., Owers, C., Horton, C., Guest, P., King, S., Williams, S., et al. (2021). National crop mapping using Sentinel-1 time series: A knowledge-based descriptive algorithm. Remote Sens., 13, 846. https://doi.org/10.3390/rs13050846

Rao, P., Zhou, W., Bhattarai, N., Srivastava, A.K., Singh, B., Poonia, S., Lobell, D.B., Jain, M. (2021). Using Sentinel-1, Sentinel-2, and Planet imagery to map crop type of smallholder farms. Remote Sensing, 13(10),1870. https://doi.org/10.3390/rs13101870

Ren, T., Xu, H., Cai, X., Yu, S., Qi, J. (2022). Smallholder crop type mapping and rotation monitoring in mountainous areas with Sentinel-1/2 imagery. Remote Sensing, 14(3), 566. https://doi.org/10.3390/rs14030566

Samberg, L.H., Gerber, J.S., Ramankutty, N., Herrero, M., West, P.C. (2016). Subnational distribution of average farm size and smallholder contributions to global food production. Environ. Res. Lett. 11(12), 124010. https://doi.org/10.1088/1748-9326/

Ricciardi, V., Ramankutty, N., Mehrabi, Z., Jarvis, L., Chookolingo, B. (2018). How much of the world's food do smallholders produce? Global Food Security, 17, 64-72. https://doi.org/10.1016/j.gfs.2018.05.002

Rufin, P., Bey, A., Picoli, M., Meyfroidt, P. (2022). Large-area mapping of active cropland and short-term fallows in smallholder landscapes using PlanetScope data. International Journal of Applied Earth Observation and Geoinformation, 112, 102937. https://doi.org/10.1016/j.jag.2022.102937

Sothe, C., Almeida, C.M., Liesenberg, V., Schimalski, M.B. (2017). Evaluating sentinel-2 and Landsat-8 data to map successional forest stages in a subtropical forest in Southern Brazil. Remote Sensing 9, 838.

Stumpf, A., Lachiche, N., Malet, J.-P., Kerle, N., Puissant, A. (2014). Active learning in the spatial domain for Remote Sensing image classification. IEEE Trans. Geosci. Remote Sensing, 52(5):2492–2507. https://doi.org/10.1109/TGRS.2013.2262052

Srivastava, A.M., Ewert, F., Akinwumiju, A.S., Zeng, W., Ceglar, A., Ezui, K.S., Adelodun, A., Adebayo, A., Sobamowo, J., Singh, M., Rahimi, J., Gaiser, T. (2023). Cassava yield gap—A model-based assessment in Nigeria. Front. Sustain. Food Syst. Sec. Agroecology and Ecosystem Services, 6. https://doi.org/10.3389/fsufs.2022.1058775

Taiwo, B.E., Al Kafy, A., Samuel, A.A., Rahaman, Z.A., Ayowole, O.E., Shahrier, M., Duti, B.M., Rahman, M.T., Peter, O.T., Abosede, O.O. (2023). Monitoring and predicting the influences of land use/land cover change on cropland characteristics and drought severity using remote sensing techniques. Environmental and Sustainability Indicators, 18, 100248. https://doi.org/10.1016/j.indic.2023.100248.

Tuia, D., Pasolli, E., Emery, W.J. (2011). Using active learning to adapt remote sensing image classifiers. Remote Sensing of Environment, 115(9):2232–2242. https://doi.org/10.1016/j.rse.2011.04.022

Veloso, A., Mermoz, S., Bouvet, A., Le Toan, T., Planells, M., Dejoux, J.F., Ceschia, E. (2017). Understanding the temporal behavior of crops using Sentinel-1 and Sentinel-2-like data for agricultural applications. Remote Sensing of Environment, 199, 415–426.

Vreugdenhil, M., Wagner, W., Bauer-Marschallinger, B., Pfeil, I., Teubner, I., Rüdiger, C., Strauss, P. (2018). Sensitivity of Sentinel-1 backscatter to vegetation dynamics: An Austrian case study. Remote Sens., 10, 1396.

Waldner, F., Diakogiannis, F.I. (2020). Deep learning on edge: Extracting field boundaries from satellite images with a convolutional neural network. Remote Sens. Environ., 245, 111741.

Wang, S., Waldner, F., Lobell, D.B. (2022). Unlocking large-scale crop field delineation in smallholder farming systems with Transfer Learning and Weak Supervision. Remote Sensing, 14(22):5738. https://doi.org/10.3390/rs14225738

Whitcraft, A.K., Vermote, E.F., Becker-Reshef, I., Justice, C.O. (2015). Cloud cover throughout the agricultural growing season: Impacts on passive optical earth observations. Remote Sens. Environ., 156, 438–447.

Web references

FAO (2015). A data portrait of smallholder farmers. https://www.fao.org/fileadmin/templates/esa/smallholders/Concept_Smallholder_Dataportrait_web.pdf [Accessed 02 Sept. 2023]

United Nations (2015). *Transforming our World: The 2030 Agenda for Sustainable Development*. A/RES/70/1. 21252030 Agenda for Sustainable Development web.pdf (un.org) [Accessed 04 Jan. 2023].

United Nations (2017). United Nations Decade of Family Farming (2019-2028). 72nd UN General Assembly. A/c.2/72/L.12/Rev1. https://digitallibrary.un.org/record/1479766 [Accessed 01 Dec. 2023].

Data references

ESA 2021. Product Validation Report (D12-PVR), WorldCover_PVR_v2. https://worldcover2021.esa.int/data/docs/WorldCover_PVR_V2.0.pdf [Accessed 01 Dec. 2023].

ESRI 2021. Living atlas https://livingatlas.arcgis.com/landcover/ [Accessed 01 Dec. 2023].

Planet Team (2022). Planet Application Program Interface: In space for life on Earth. San Francisco, CA. https://api.planet.com [Accessed 06 Jan. 2023].

Planet-NICFI (2023). Norway's International Climate and Forest Initiative Satellite program collection. https://www.planet.com/nicfi/ [Accessed 06 Jan. 2023].